Transport into Nanosheets: Diffusion Equations Put to Test

Nils E. R. Zimmermann,* Timm J. Zabel, and Frerich J. Keil

Institute for Chemical Reaction Engineering, Hamburg University of Technology, Eissendorfer Str. 38, 21073 Hamburg, Germany

E-mail: nils.zimmermann@tu-harburg.de

*To whom correspondence should be addressed

Abstract

Ultrathin porous materials, such as zeolite nanosheets, are prominent candidates for performing catalysis, drug supply, and separation processes in a highly efficient manner due to exceptionally short transport paths. Predictive design of such processes requires the application of diffusion equations that were derived for macroscopic, homogeneous surroundings to nanoscale, nano-structured host systems. Therefore, we tested different analytical solutions of Fick's diffusion equations for their applicability to methane transport into two different zeolite nanosheets (AFI, LTA) under instationary conditions. Transient molecular dynamics simulations provided hereby concentration profiles and uptake curves to which the different solutions were fitted. Two central conclusions were deduced by comparing the fitted transport coefficients. First, the transport can be described correctly only if concentration profiles are used and the transport through the solid-gas interface is explicitly accounted for by the surface permeability. Second and most importantly, we have unraveled a size limitation to applying the diffusion equations to nanoscale objects. This is because transport-diffusion coefficients, D_{T}, and surface permeabilities, α, of methane in AFI become dependent on nanosheet thickness. Deviations can amount to factors of 2.9 and 1.4 for D_{T} and α, respectively, when, in the worst case, results from the thinnest AFI nanosheet are compared with data from the thickest sheet. We present a molecular explanation of the size limitation that is based on memory effects of entering molecules and therefore only observable for smooth pores such as AFI and carbon nanotubes. Hence, our work provides important tools to accurately predict and intuitively understand transport of guest molecules into porous host structures, a fact that will become the more valuable the more tiny nanotechnological objects get.

Introduction

Fueled by recent synthesis breakthroughs,[1] nano-scale objects, such as nanosheets,[1–5] nanoflakes,[6] and nanotubes,[7] have attracted the attention of many scientists and engineers in the past decade. The interest is based mainly on two factors. On the one hand, the materials forming nanoobjects serve as catalysts,[1] drug supply systems,[2] adsorbents,[3] energy storage media,[4,5] thermoelectric elements,[6] and gas sensing devices,[7] thus opening abundant application possibilities. On the other hand, fabricating the materials as small as possible is critical to almost any of the processes to be performed as efficient as possible. This is because molecular transport of guest species – reactants/products,[1,8] drugs,[2] dyes,[3] ions,[4,5] and gas molecules,[7] – into or through the solid turns out to be a crucial, if not the rate-limiting step[7,8] of many of the above processes. Reducing the dimensions of the porous host structure and thereby the diffusion path of the guest species is therefore the most direct means to increase apparent reaction rates,[1,8] decrease detection[7] and recharge[5] times, and thus optimize the process efficiency.[4]

Transport into porous materials[9–11] is usually described by Fick's laws[12]

$$j(z) = -D_{\mathrm{T}} \times \frac{\mathrm{d}c(z)}{\mathrm{d}z} \tag{1}$$

$$\frac{\partial c(t,z)}{\partial t} = D_{\mathrm{T}} \times \frac{\partial^2 c(t,z)}{\partial z^2} \tag{2}$$

These well-known equations connect the transport flux, j, with the driving force, $-\mathrm{d}c(z)/\mathrm{d}z$, via the transport-diffusion coefficient, D_{T}, state how concentration fluctuations decay with time t, and are strictly speaking valid for constant diffusivities only. While special transport problems might require suitable extensions and adaptations, for example, Maxwell-Stefan formulation for multicomponent diffusion[13] and extra adsorption terms for strongly interacting guest-host systems,[14] single-component transport of hydrocarbons into zeolites is well described by Fick's laws.[9,11] However, since these equations were derived under specific assumptions[15] and applied to rather large crystals[9–11] two critical issues appear for novel nano-scale host structures.

The first one is a consequence of the host materials' periodic structure, where we will focus on

zeolites in the following. The discrete subunits that build up the host crystal (i.e., cages of the unit cell) contrast a main assumption upon which the diffusion equations were derived:[15] a structureless homogeneous continuum. However, as long as the host structure is large, ideally consisting of an infinite number of cages, previous efforts, by means of simulations[13] and experiments,[9–11] have shown that the conventional equations are well applicable to describe guest molecule transport. But what happens when the size of the material leaves the macro and microscale to reach just some nanometers? Are the diffusion equations still valid and reliable at this small scale?

Second, the role of the interface between gas space and "bulk" host interior is often assumed to be negligible. In this respect, cases have been identified where the interface exhibited very similar[10,11] transport characteristics as the bulk host structure, influenced only by the number of blocked pore entrances.[11] However, we have recently shown[16] that this is not generally true. The transport coefficient at the interface, the so-called surface permeability α, varied in a distinctly different manner with loading in our study than the diffusivity.[16] So, in which cases does the surface permeability correlate with the diffusion coefficient?[17] And, is this relevant to processes implementing nanosheets or ultrathin membranes?[18]

Given the problems outlined, here we test the validity of Fick's diffusion equations and their existing analytical solutions to guide future process design improvements in nanotechnology. For this purpose, the dynamics of methane transport into initially empty zeolite nanosheets was studied until saturation was reached. Transient molecular dynamics simulations[19] were employed, and we focused on three factors:

1. type of analytical solution of diffusion equations (local vs integral),
2. role of boundary conditions (surface-barrier effects), and
3. influence of sheet thickness ("nano effect").

Two zeolite types were investigated: an AFI-type zeolite (Figure 1a) with smooth one-dimensional channels, and an LTA zeolite which possesses bulky cages connected via narrow pore windows (Figure 1c). The respective external surfaces of the two zeolites are depicted in Figure 1b and d.

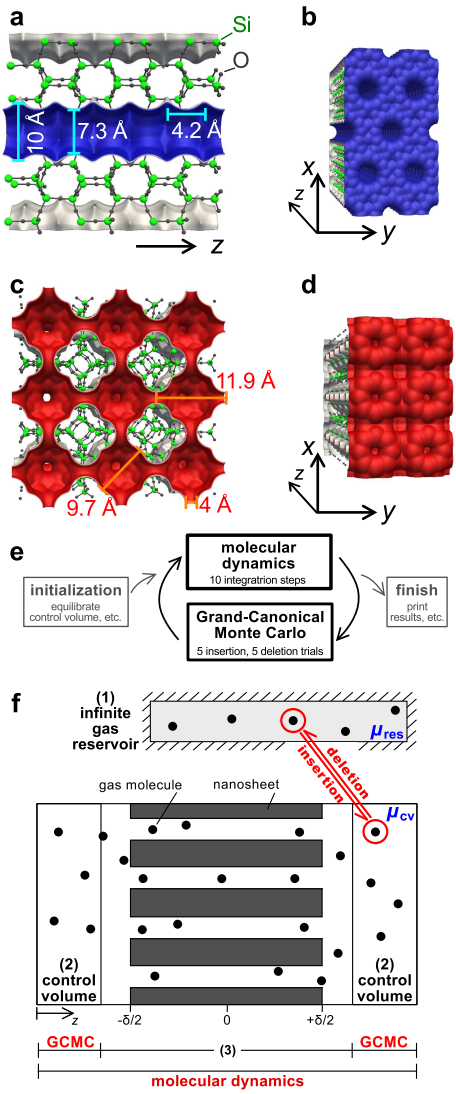

Figure 1: Representations of zeolite nanosheets investigated and their external surface: AFI (a,b) and LTA (c,d). Schemes illustrating the alternating GCMC-MD procedure in a transient molecular dynamics calculation (e) and important spatial regions (f): The hypothetical gas reservoir (1) exchanges molecules with the control volume [CV (2)] via GCMC trials to maintain CV's chemical potential because once outside the CV (3) the molecules cannot be deleted from the box anymore.

Methodology

Transient molecular dynamics (TrMD), which is also referred to as non-equilibrium molecular dynamics (NEMD),[19] represents a subtype of conventional equilibrium molecular dynamics (EMD).[20] Both simulation methods determine the evolution of a many-molecule system via numerical solution of Newton's equations of motion.[21] The difference lies in the fact that TrMD allows for a varying number of molecules, N, in the simulation box whereas N is strictly constant in EMD. Variation of the number of molecules is achieved by executing, in an alternating manner, conventional MD integration steps and Grand-Canonical Monte Carlo (GCMC) trials, as depicted in Figure 1e. Importantly, all molecules are subject to MD irrespective of their positions (Figure 1f). However, molecules are restricted to be inserted into and deleted from a specific region of the simulation box via GCMC: the control volume (CV). GCMC trials mimic therefore exchange with a hypothetical, infinite gas reservoir whose chemical potential, μ_{res}, is identical to the one imposed on the control volume, μ_{cv}. Thus, the control volume is automatically replenished with molecules once too many have left the CV to maintain μ_{cv}. Molecules outside the CV may now enter the zeolite that was initially empty.

In the present paper, the gradual filling of the nanosheet with methane molecules is monitored in two ways during a TrMD simulation. First, concentration profiles, $c(t_i, z_k)$, are determined across the sheet (i.e., along z) at successive times t_i. This approach will be referred to as *local* in the remainder. Second, an uptake curve,[16,22,23] $m(t_i)$, is calculated on the basis of the concentration profiles which describes the increase of the total mass adsorbed inside the nanosheet as a function of time. Since an uptake curve is, by definition, spatially not resolved we call it an *integral* approach to monitor the transport process. Notice that such integral solutions of the diffusion equations are important because they are central functions in both diffusion experiment evaluation[22] and process design.[23,24] More details on the simulations[19] and an in-depth discussion about the models used[25–29] are presented in the Supporting Information (SI1 and SI2.1). It is, at this point, important to emphasize that molecular simulations are the methods of choice for this study. To the best of our knowledge, there is presently no measurement technique that has both the

necessary spatial and temporal resolution to directly monitor local molecular uptake inside porous nanosheets and thus being capable of checking the validity of Fick's diffusion equations for guest transport into nano-scale host materials. Furthermore, note that the here employed computationally demanding non-equilibrium methodology[19] and a similar approach[30] have so far been used to assess surface transport resistances only. Hence, the crucial difference to previous works[19,30] is the simultaneous occurrence of surface and intracrystalline transport resistances.

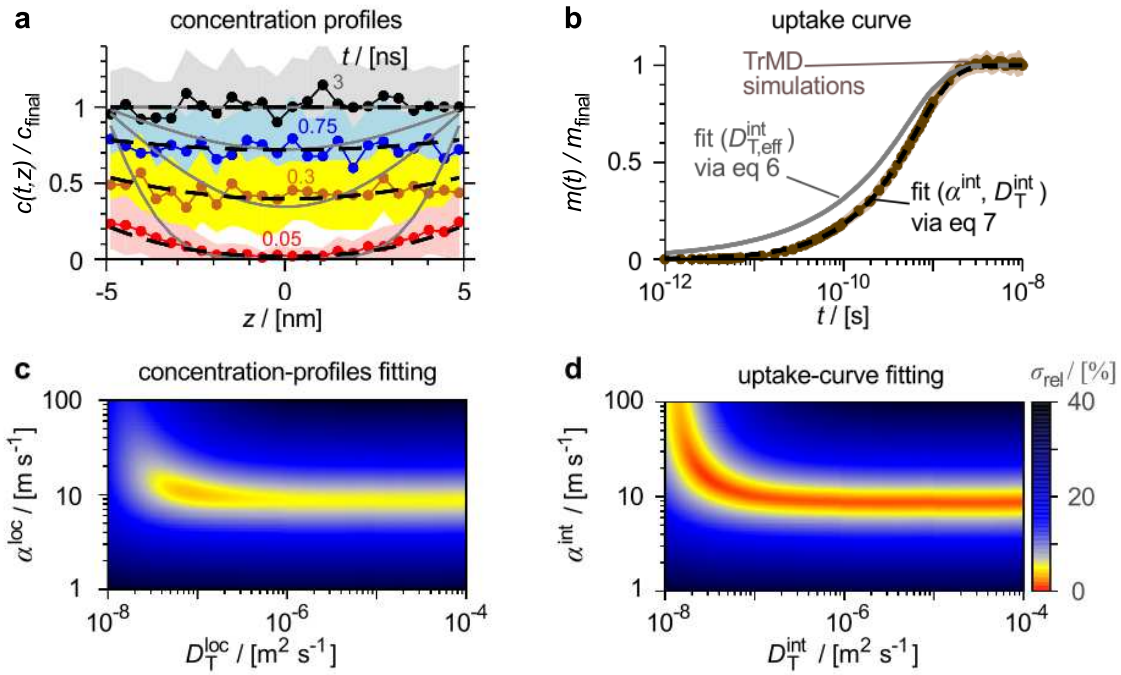

Figure 2: Relative concentration profiles, $c(t,z)/c_{\text{final}}$, and the resulting uptake curve, $m(t)/m_{\text{final}}$, from transient MD (dots connected with solid lines in a and b) for methane entering a 10.2 nm AFI nanosheet at 300 K. Acceptable noise was achieved by performing 40 independent transient MD runs over which the profiles were averaged. Therefore, colored domains indicate the statistical spread. Grey solid lines in Figure 2a represent the best fit of eq 4 by variation of $D_{\text{T,eff}}^{\text{loc}}$ to the TrMD data whereas dashed lines correspond to results of fitting c-profiles via α^{loc} and $D_{\text{T}}^{\text{loc}}$ (eq 5). Likewise, the grey line in Figure 2b is the result of fitting the uptake curve via $D_{\text{T,eff}}^{\text{int}}$ to the TrMD curve (eq 6), and the dashed line is the best fit of eq 7 by variation of α^{int} and $D_{\text{T}}^{\text{int}}$. The parameter spaces, $\sigma_{\text{rel}}(D_{\text{T}},\alpha)$, for the solutions with surface permeability are highlighted in parts c and d. They depict the agreement between TrMD data and analytical solutions of the diffusion equations in dependence of parameters D_{T} and α. Red areas indicate good agreement whereas black regions correspond to large deviations.

Figure 2 shows typical concentration profiles (a) and an uptake curve (b), both obtained from

TrMD simulations of methane entering a δ =10.2 nm thick AFI sheet (dots connected with lines). The temperature was 300 K and the chemical potential in the control volume corresponded to 10 bar of gas-phase pressure. The concentration profiles and the uptake curve from TrMD were then used to fit analytical solutions of the diffusion equations provided by Crank for a plane sheet.[15] Two analytical solutions were investigated per approach (i.e., local via *c*-profiles and integral via uptake curves) which differed in their boundary conditions. The first one assumes that the transport at the solid-gas interface proceeds extremely fast such that the final equilibrium concentration, c_{final}, is attained instantaneously at the sheet boundaries. In that case, a single parameter, the effective transport-diffusion coefficient $D_{\text{T,eff}}$, describes the entire process. The second boundary condition models finite transport through the solid-gas boundary layer by introducing a second transport parameter in addition to the transport-diffusivity D_{T}: the surface permeability α. It links the instantaneous guest flux, $j(t,\pm\delta/2)$, at time t across the boundary layers at $z=\pm\delta/2$ (right and left sheet surfaces) with the driving concentration difference via

$$j(t,\pm\delta/2) = \alpha \times [c(t,\pm\delta/2) - c_{\text{final}}]. \tag{3}$$

Four analytical solutions were hence investigated in this work.[15]

Concentration profiles derived by neglecting surface barriers at the sheet entrances represent the first type of analytical solutions investigated:

$$\frac{c(t,z)}{c_{\text{final}}} = 1 - \frac{4}{\pi}\sum_{i=0}^{\infty}\left\{\frac{(-1)^i}{2i+1} \times \exp[-D_{\text{T,eff}}^{\text{loc}}(2i+1)^2\pi^2 t/\delta^2] \times \cos\frac{(2i+1)\pi z}{\delta}\right\} \tag{4}$$

where δ is the thickness of the nanosheet. Note that superscripts of transport coefficients indicate in the following the solution type to which the coefficients were fitted (concentration profiles: "loc" for local; uptake curves: "int" for integral). Furthermore, subscript "eff" signifies cases in which the diffusion coefficients capture in effect both transport resistance types: diffusion barriers caused by the repetitive zeolite structure[31,32] and surface barriers at the zeolite-gas boundary layer.[16,23,33]

Concentration profiles (superscript "loc") derived with the surface-barrier boundary condition

by introduction of α are the second type of solutions:

$$\frac{c(t,z)}{c_{\text{final}}} = 1 - \sum_{i=1}^{\infty} \left\{ \frac{2L \times \exp[-\gamma_i^2 D_{\text{T}}^{\text{loc}} t/(\delta/2)^2]}{(\gamma_i^2 + L^2 + L)\cos\gamma_i} \times \cos[\gamma_i z/(\delta/2)] \right\} \tag{5}$$

Here, γ_i is the i-th positive root of $\gamma \tan\gamma = L$ with $L = (\delta/2)\alpha^{\text{loc}}/D_{\text{T}}^{\text{loc}}$ where we have omitted superscript "loc" of γ and L in eq 5 for reasons of clarity.

Uptake curves (superscript "int") derived by neglecting surface barriers at the sheet entrances (subscript "eff") represent the third analytical solution type

$$\frac{m(t)}{m_{\text{final}}} = 1 - \sum_{i=0}^{\infty} \frac{8 \times \exp[-D_{\text{T,eff}}^{\text{int}}(2i+1)^2\pi^2 t/\delta^2]}{(2i+1)^2\pi^2} \tag{6}$$

where m_{final} denotes the final mass after saturation of the nanosheet with guest molecules.

Finally, uptake curves (superscript "int") derived with the surface-barrier boundary condition are the fourth type of solutions:

$$\frac{m(t)}{m_{\text{final}}} = 1 - \sum_{i=1}^{\infty} \frac{2L^2 \times \exp[-\gamma_i^2 D_{\text{T}}^{\text{int}} t/(\delta/2)^2]}{\gamma_i^2(\gamma_i^2 + L^2 + L)} \tag{7}$$

where again γ_i is the i-th positive root of $\gamma \tan\gamma = L$, however, with $L = (\delta/2)\alpha^{\text{int}}/D_{\text{T}}^{\text{int}}$.

We have included the results of fitting the four different analytical solutions in Figure 2a and b for the given example. Parts c and d of Figure 2 highlight the parameter spaces of the analytical solutions with the surface-barrier boundary condition. That is, the averaged relative sample standard deviation, σ_{rel} in [%], in dependence of transport coefficients D_{T} and α. The averaged relative sample standard deviation is hereby defined as

$$\sigma_{\text{rel}}(D_{\text{T}}^{\text{loc}}, \alpha^{\text{loc}})/[\%] \equiv 100 \sqrt{1/(N_t N_z) \times \sum_{i}^{N_t} \sum_{k}^{N_z} \left[c(D_{\text{T}}^{\text{loc}}, \alpha^{\text{loc}}, t_i, z_k) - \bar{c}(t_i, z_k) \right]^2} / c_{\text{final}} \tag{8}$$

where N_t and N_z denote respectively the (discrete) number of time instances and the number of points in the concentration profiles and $c(D_{\text{T}}^{\text{loc}}, \alpha^{\text{loc}}, t_i, z_k)$ the concentration value from the analyt-

ical solution (here: eq 5) at time t_i and position z_k. Note that the corresponding concentration from TrMD is an average $[\bar{c}(t_i, z_k)]$ because 40 independent TrMD simulations were required to yield profiles with acceptable noise. The definition of σ_{rel} for uptake-curve fitting is similar, with the difference that one does not need to average over spatial points N_z:

$$\sigma_{\mathrm{rel}}(D_{\mathrm{T}}^{\mathrm{int}}, \alpha^{\mathrm{int}})/[\%] \equiv 100 \sqrt{1/N_t \times \sum_{i}^{N_t} \left[m(D_{\mathrm{T}}^{\mathrm{int}}, \alpha^{\mathrm{int}}, t_i) - \bar{m}(t_i) \right]^2 / m_{\mathrm{final}}} \tag{9}$$

Results

Figure 2 shows that the analytical solutions of the diffusion equations which are based exclusively on the effective diffusivity (grey solid lines in Figure 2a and b) cannot accurately reproduce neither the concentration profiles nor the uptake curve from transient MD. That is particularly evident at early stages and the outermost region of the *c*-profiles. The shortcoming of describing the TrMD data is quantitatively reflected in an increasing effective diffusivity with sheet thickness δ, as seen in Table 1, because diffusion coefficients must theoretically not depend on primary geometrical parameters. We observe an increasing diffusivity for both solution types, local and integral, and for both zeolites, AFI and LTA. Since it is well-known that adsorbate diffusion coefficients in zeolites can exhibit strong concentration dependencies[13,28] we have determined methane transport-diffusivities using conventional EMD simulations in periodic crystals (SI2.2). The transport-diffusivities were averaged over the concentration range relevant to our TrMD simulations ($\bar{D}_{\mathrm{T}}$) and amounted to 755×10^{-10} m^2/s and 9.2×10^{-10} m^2/s for AFI and LTA, respectively. The effective diffusion coefficients $D_{\mathrm{T,eff}}^{\mathrm{loc}}$ and $D_{\mathrm{T,eff}}^{\mathrm{int}}$ in Table 1 asymptotically approach the concentration-averaged values from EMD with increasing sheet thickness which proceeds faster for LTA than for AFI. Therefore, we conclude that the quality of describing guest transport on the basis of diffusion coefficients alone, that is, by neglecting the influence of surface barriers altogether, worsens the smaller the host dimension becomes and the larger the average guest diffusivity is.

Those two analytical solutions that account for possible surface barriers through the surface permeability α yield excellent agreement with the simulation data (dashed lines in Figure 2a and b). In fact, the concentration profiles' shape and evolution, very flat lines that gradually shift towards the equilibrium value, are already clear indicators of strong surface barriers,[17] and they resemble profiles obtained from interference microscopy (IFM) experiments on giant crystals.[10,11] The difference to the experiments lies in the complementary nature of the barrier types probed. While IFM measurements detect blocked pore entrances and therefore "departure" from the ideal crystal surface,[10,11,17] we measure crystal-structure inherent surface barriers.[16] Importantly, both methods for assessing surface barriers have their drawbacks. IFM measurements alone cannot provide the reason to pore blockage (e.g. foreign matter, lattice dislocations, surface reconstruction) and our results provide only a lower bound to surface barriers because of the highly idealized nature of the structures employed.

Table 1: Diffusion Coefficients[a] and Surface Permeabilities[b]

	δ [nm]	$D_{T,eff}^{int}$ [10^{-10}m^2/s]	σ_{rel} [%]	$D_{T,eff}^{loc}$ [10^{-10}m^2/s]	σ_{rel} [%]	α^{int} [m/s]	D_{T}^{int} [10^{-10}m^2/s]	σ_{rel} [%]	α^{loc} [m/s]	D_{T}^{loc} [10^{-10}m^2/s]	σ_{rel} [%]
AFI[c]	2.6	38	6.6	43	16	10.8	15200	2.6	11.0	2319	3.9
	5.1	73	5.5	78	16	13.6	328	1.9	11.1	1065	3.9
	10.2	124	4.7	137	16	15.5	313	0.9	10.5	835	3.6
	20.4	175	4.3	189	16	13.7	375	0.4	8.8	868	3.3
	40.7	263	3.9	284	14	11.4	490	0.4	7.8	798	3.4
LTA[d]	4.8	1.29	9.4	1.40	11	0.200	8850	4.1	0.262	6.5	5.1
	11.9	3.08	8.2	2.88	13	0.198	21900	2.2	0.294	10.5	4.3
	26.1	4.94	5.2	4.61	11	0.210	18.1	0.8	0.340	8.9	3.6

[a]EMD: $\bar{D}_T = 755 \times 10^{-10}$ m^2/s (AFI) and 9.2×10^{-10} m^2/s (LTA); note that fitting eq 5 via a concentration-dependent transport-diffusivity gives very similar values for $\bar{D}_T^{loc}$ (SI4). [b]MC: $\bar{\alpha}_S = 7.6$ m/s (AFI) and 0.383 m/s (LTA). [c]T=300 K, $p(\mu_{cv})$=10 bar. [d]T=750 K, $p(\mu_{cv})$=100 bar; note that elevated temperature and pressure were required for TrMD simulations of CH_4 in LTA as discussed in SI1.1.

Despite the good agreement between both analytical solutions using the surface-barrier boundary conditions and TrMD simulation data, the corresponding fitted transport coefficients reveal two peculiarities (Table 1). First, diffusion coefficients determined by the integral solution deviate strongly from the EMD concentration-averaged value, $\bar{D}_T$, but, interestingly, in different manners for the two zeolites. In contrast to AFI, for which the fitted values (D_T^{int}) are smaller than $\bar{D}_T$ by a factor of two on the average, fitted LTA diffusivities are, on average, 1000 times larger than $\bar{D}_T$. Note that we consider D_T^{int} obtained from the thinnest AFI sheet as an outsider for reasons given below (second peculiarity). However, using concentration profiles to describe the transport (D_T^{loc}) yields a good match between TrMD and EMD data. This implies that accurate modeling of guest transport into nano-scale host materials is achieved only by spatially resolved analytical solutions of the diffusion equations. The argument is all the more valid as we have similar indication from the surface permeability.

Only recently, we have provided an accurate prediction of the surface permeability,[16] α_S, which applies to tracer-exchange and thus self-diffusion situations, hence subscript "S". Using the data from ref 16 for AFI and calculating fresh tracer-exchange surface permeabilities for methane in LTA (SI3), we obtain concentration-averaged values, $\bar{\alpha}_S$, of 7.6 m/s and 0.383 m/s, being in good agreement with the values from fitting concentration profiles (α^{loc} in Table 1). However, surface permeabilities from fitting uptake curves (α^{int}) tend to over- and underrate the equilibrium simulation prediction $\bar{\alpha}_S$ by average factors of 1.8 and 1.9 for AFI and LTA, respectively, which we regard as further evidence of the inappropriateness of using uptake curves.

Finally, the parameter spaces are also indicative of the problem because a well-localized minimum of $\sigma_{rel}(D_T^{loc}, \alpha^{loc})$ is observed for *c*-profile fitting (orange region in Figure 2c). By contrast, the optimum parameter region of the integral solution is very flat and L-shaped, indeed stretching along the axis of both parameters as a red stripe in Figure 2d (note the several orders of magnitude displayed for D_T^{int}). Therefore, if one were to use integral analytical solutions of the diffusion equations to analyze guest transport data[16,22] in nano-scale host objects by applying automatic optimization algorithms our results give clear evidence that care must be taken because such al-

gorithms are prone to oscillations in flat parameter spaces.

The deficiency of uptake curves to accurately describe the transport progress into nanoscale objects may be grounded on the statistical noise of the TrMD data. Our previous work on tracer-exchange transport[16] has shown that diffusivities and surface permeabilities are generally extractable from uptake curves when the data exhibit virtually no statistical noise. The analysis of our TrMD simulations was indicative of decreasing noise with increasing sheet thickness. For this reason, we think that once the noise has fallen below a certain threshold it is possible that the transport coefficients obtained from uptake-curve and concentration-profile fitting, respectively, will agree with one another. This, however, would be observable above a "threshold" thickness only.

Focusing in the remainder on the spatially resolved surface-barrier model for the reasons given above, the second peculiarity deduced from the fitted transport data lies in the following. AFI diffusion coefficients, $D_{\mathrm{T}}^{\mathrm{loc}}$, and surface permeabilities, α^{loc}, distinctly decrease with increasing sheet thickness. They slowly approach the (concentration-wise averaged) values from EMD simulations where the deviation between the thinnest sheet and EMD values amount to factors of 3 and 1.5 for $D_{\mathrm{T}}^{\mathrm{loc}}$ and α^{loc}, respectively. The diffusivity deviations are in fact such strong that, except for the thickest nanosheet, all $D_{\mathrm{T}}^{\mathrm{loc}}$ exceed the maximum D_{T} from EMD in the concentration range of interest, which clearly highlights that the concentration dependence of the diffusion coefficient cannot be the reason for the deviations. The trend is however entirely absent for LTA. In a previous work,[16] we have observed a similar decrease of methane-tracer diffusion coefficient with AFI sheet thickness. In that case, we could attribute the decrease to the influence of lower methane adsorption in the solid-gas interface region as compared to the adsorption in the bulk solid space.[16,34] For this study, however, we circumvented this influence by excluding the interface region (external surface-adsorption layer and outermost zeolite cage) from the concentration profiles that were fitted to the analytical solutions (SI1.1). Therefore, the origin of decreasing diffusion coefficients in AFI must have other reasons. We hypothesize that this is indeed owing to the exceptionally thin host structure in conjunction with the shape of the pores.

To understand the mechanism behind our hypothesis, consider a single molecule entering an empty nanopore (Figure 3). That situation is encountered at early stages in our TrMD simulations. In the case of LTA, a molecule that has just entered the first cage (Figure 3a) will immediately loose its memory where it came from because of high entropic diffusion barriers.[31] The quick loss of memory is a prerequisite for applying random-walk theory on the length scale of a single zeolite cage. The smooth AFI pore shape (Figure 3b), on the other hand, does not cause as large diffusion barriers between adjacent cages as in LTA. Because of the low barriers which range around $1k_BT$,[28,32] the molecule is unlikely to equilibrate in the first cage and jumps immediately into the next cage and even further to undertake a cascade of jumps. As a result of these multi-jumps,[32] the diffusivity, at low loading, is higher compared to free-energy barrier estimates. This phenomenon, called kinetic jump correlations,[32,35] implies that whilst random walk theory is not applicable on the length scale of a *single cage* it just takes the molecule more time and therefore a longer distance to loose its memory where it came from.[36] Absence of any systematic deviation of the mean-squared displacement (MSD) from ideal self-diffusion behavior,[28] that is, MSD $\propto t$, serves yet as strong evidence of the existence of an underlying Markovian chain on *some* length scale. Obviously, the smallest sheet thicknesses used in our TrMD simulations are just within this "randomization" length scale because the first molecules entering the sheet at low concentrations do not have enough time to loose their memory. This gives rise to faster filling and thus larger diffusivities with decreasing sheet dimension. We attribute the similar though more subtle trend for the surface permeability, α^{loc}, to exactly the same reason. Crucially, this "nano effect" manifests a size limitation to describing guest transport into porous materials with Fick's laws in such a sense that the transport coefficients depend on the geometrical parameters of the host.

As mentioned earlier, interference[11] and infrared[10,11] microscopy measurements have unraveled that the transport-diffusivity and the surface permeability of hydrocarbons follow the same concentration dependence in the case of the metal-organic framework Zn(tbip) and zeolite $AlPO_4$-LTA. However, we have recently shown[16] that this correlation[17] between the two transport coefficients is not unique. While the tracer-exchange surface permeability, α_S, of methane in AFI

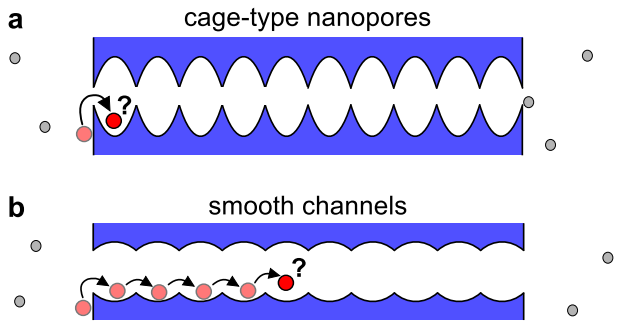

Figure 3: A molecule (red circle) looses its memory immediately provided it enters a cage-type zeolite pore (a). If the pores are however rather smooth (b) the molecule will have a high likelihood to perform a series of multi-jumps over several cages until it "forgets" where it came from.

increased with concentration, the self-diffusivity decreased.[16] Here, we can directly compare the permeability-to-diffusivity ratio over concentration for AFI and LTA using the data from equilibrium molecular simulations (SI3). As seen from Figure 4, α_S correlates with D_S in the case of LTA but not for AFI where the permeability is markedly smaller than the diffusivity. The correlation might lead to the impression that surface barriers are not important to methane transport into LTA nanosheets[23] because α_S and D_S are alike. However, recall that increasing the thickness of the LTA nanosheet by a factor of 5.4 yields a 3.3 times larger effective transport-diffusivity (Table 1) which is still only half of the true transport-diffusivity D_T^{loc}. Hence, accurate modeling of molecular transport into nanosheets always needs to employ the surface-barrier boundary condition which is due only to the exceptional small thickness of the host material.

Conclusions

Three central consequences follow from our results to predictive process design where guest transport into nanoobjects plays a critical role. First, we have clearly shown the imperative of modeling transport with spatially-resolved models (*c*-profiles) that are grounded on an explicit description of the transport in the boundary layer between sheet and bulk fluid phase (α), irrespective of the guest-host match.[23,29] Second, our work indicates that rapid equilibrium simulations can be used to predict both the diffusion coefficient[13] and the surface permeability,[16] provided that the sheet

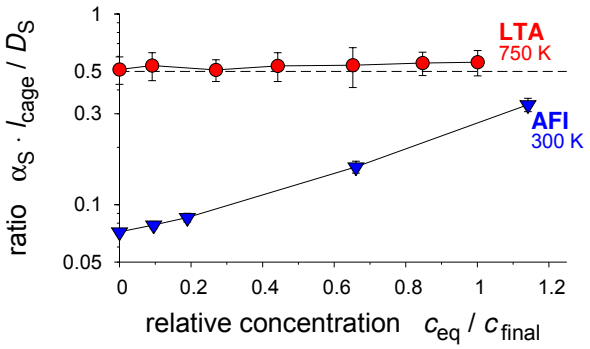

Figure 4: Ratio of methane-tracer surface permeability,[16] α_S, to diffusivity, D_S, normalized by distance l_{cage} and plotted as a function of relative concentration, c_{eq}/c_{final}, for the two zeolite materials studied. Note that the subscript "eq" signifies that the data and thus the concentration dependence was obtained from equilibrium molecular simulations and not from TrMD simulations.

thicknesses are larger than 100 nm or guest diffusivities lower than $\approx 10^{-8}$ m^2/s. Rare event techniques[37] and histogram re-weighting methods[38] may in this context be used to push the prediction range even further to cases of extremely high diffusion and surface barriers. This may ultimately permit automated[39] high throughput in-silico screening studies[40] to account also for (surface) transport influences. However, we need to point out that we have investigated *single*-component transport only. Most applications[2–5,7] have yet to deal with a mixture of various guest species. It will hence be necessary to test the applicability and predictability of the surface permeability in *multi*-component situations, too. Incorporation into the Maxwell-Stefan formulation[8,13] seems to be a valuable starting point which, in our opinion, represents one of the future key challenges in diffusion theory in order to meet the needs of nanotechnology from a process design perspective. Third, we have detected a limitation to applying Fick's laws to nano-scale objects which is due to the combination of their exceptional size and memory effects of the diffusing guest molecules. Owing to the crucial role of nanopore shape, we expect that this phenomenon will be even stronger in carbon nanotubes than in the AFI-type zeolite studied here. This would, for example, imply that predictive design of future gas-sensing devices[7] needs to account for CNT-length dependent diffusion coefficients, in the context of which transient molecular dynamics[19] will be a useful complementary design tool.

Acknowledgment

We dedicate this paper to Dr. Siegfried Fritzsche for his inspiring contributions to computational zeolite science. Furthermore, we thank Dr. Sven Jakobtorweihen for critical reading of the manuscript. The authors acknowledge financial support by the German Research Foundation [Deutsche Forschungsgemeinschaft (DFG)] in priority program SPP 1155 under contract KE 464/10-1.

Associated Content

Supporting Information Available: Details on simulation methodology including parameter tests and model verification, complementary results of surface permeabilities and concentration-dependent diffusivities, crystal structures, lists of symbols and abbreviations; movie illustrating TrMD (butane in AFI). This information is available free of charge via the Internet at http://pubs.acs.org.

References

(1) Choi, M.; Na, K.; Kim, J.; Sakamoto, Y.; Terasaki, O.; Ryoo, R. *Nature* **2009**, *461*, 246–249.

(2) Wheatley, P. S.; Butler, A. R.; Crane, M. S.; Fox, S.; Xiao, B.; Rossi, A. G.; Megson, I. L.; Morris, R. E. *J. Am. Chem. Soc.* **2006**, *128*, 502–509.

(3) Song, Z.; Chen, L.; Hu, J.; Richards, R. *Nanotechnology* **2009**, *20*, year.

(4) Chen, J. S.; Tan, Y. L.; Li, C. M.; Cheah, Y. L.; Luan, D.; Madhavi, S.; Boey, F. Y. C.; Archer, L. A.; Lou, X. W. *J. Am. Chem. Soc.* **2010**, *132*, 6124–6130.

(5) L. Ren and Y. Liu and X. Qi and K. S. Hui and K. N. Hui and Z. Huang and J. Li and K. Huang and J. Zhong, *J. Mater. Chem.* **2012**, *22*, 21513–21518.

(6) Coleman, J. N. et al. *Science* **2011**, *331*, 568–571.

(7) Mirica, K. A.; Weis, J. G.; Schnorr, J. M.; Esser, B.; Swager, T. M. *Angew. Chem., Int. Ed.* **2012**, *51*, 10740–10745.

(8) Hansen, N.; Krishna, R.; van Baten, J. M.; Bell, A. T.; Keil, F. J. *J. Phys. Chem. C* **2009**, *113*, 235–246.

(9) Heinke, L.; Kortunov, P.; Tzoulaki, D.; Kärger, J. *Phys. Rev. Lett.* **2007**, *99*, 228301.

(10) Hibbe, F.; Chmelik, C.; Heinke, L.; Pramanik, S.; Li, J.; Ruthven, D. M.; Tzoulaki, D.; Kärger, J. *J. Am. Chem. Soc.* **2011**, *133*, 2804–2807.

(11) Hibbe, F.; Caro, J.; Chmelik, C.; Huang, A.; Kirchner, T.; Ruthven, D.; Valiullin, R.; Kärger, J. *J. Am. Chem. Soc.* **2012**, *134*, 7725–7732.

(12) Fick, A. *Annal. der Phys.* **1855**, *170*, 59–86.

(13) Krishna, R. *Chem. Soc. Rev.* **2012**, *41*, 3099–3118.

(14) Han, S.; Hermans, T. M.; Fuller, P. E.; Wei, Y.; Grzybowski, B. A. *Angew. Chem., Int. Ed.* **2012**, *51*, 2662–2666.

(15) Crank, J. *The Mathematics of Diffusion*, 2nd ed.; Oxford University Press: New York, USA, 1975.

(16) Zimmermann, N. E. R.; Smit, B.; Keil, F. J. *J. Phys. Chem. C* **2012**, *116*, 18878–18883.

(17) Heinke, L.; Kärger, J. *Phys. Rev. Lett.* **2011**, *106*, 074501.

(18) Veziri, C. M.; Palomino, M.; Karanikolos, G. N.; Corma, A.; Kanellopoulos, N. K.; Tsapatsis, M. *Chem. Mater.* **2010**, *22*, 1492–1502.

(19) Thompho, S.; Chanajaree, R.; Remsungnen, T.; Hannongbua, S.; Bopp, P. A.; Fritzsche, S. *J. Phys. Chem. A* **2009**, *113*, 2004–2014.

(20) Alder, B. J.; Wainwright, T. E. *J. Chem. Phys.* **1959**, *31*, 459–466.

(21) Frenkel, D.; Smit, B. *Understanding Molecular Simulations: From Algorithms to Applications*; Academic Press: San Diego, USA, 2002.

(22) F. Hibbe and V. R. R. Marthala and C. Chmelik and J. Weitkamp and J. Kärger, *J. Chem. Phys.* **2011**, *135*, 184201.

(23) Zimmermann, N. E. R.; Balaji, S. P.; Keil, F. J. *J. Phys. Chem. C* **2012**, *116*, 3677–3683.

(24) Ruthven, D. M.; Farooq, S.; Knaebel, K. S. *Pressure Swing Adsorption*; VCH Publishers: New York, USA, 1994.

(25) S. Qiu and W. Pang and H. Kessler and J. L. Guth, *Zeolites* **1989**, *9*, 440–444.

(26) Corma, A.; Rey, F.; Rius, J.; Sabater, M. J.; Valencia, S. *Nature* **2004**, *431*, 287–290.

(27) Dubbeldam, D.; Calero, S.; Vlugt, T. J. H.; Krishna, R.; Maesen, T. L. M.; Beerdsen, E.; Smit, B. *Phys. Rev. Lett.* **2004**, *93*, 088302.

(28) Zimmermann, N. E. R.; Jakobtorweihen, S.; Beerdsen, E.; Smit, B.; Keil, F. J. *J. Phys. Chem. C* **2007**, *111*, 17370–17381.

(29) Zimmermann, N. E. R.; Haranczyk, M.; Sharma, M.; Liu, B.; Smit, B.; Keil, F. J. *Mol. Simul.* **2011**, *37*, 986–989.

(30) Combariza, A. F.; Sastre, G. *J. Phys. Chem. C* **2011**, *115*, 13751–13758.

(31) Beerdsen, E.; Dubbeldam, D.; Smit, B. *Phys. Rev. Lett.* **2006**, *96*, 044501.

(32) Dubbeldam, D.; Beerdsen, E.; Vlugt, T. J. H.; Smit, B. *J. Chem. Phys.* **2005**, *112*, 224712.

(33) Zimmermann, N. E. R.; Smit, B.; Keil, F. J. *J. Phys. Chem. C* **2010**, *114*, 300–310.

(34) García-Pérez, E.; Schnell, S. K.; Castillo, J. M.; Calero, S.; Kjelstrup, S.; Dubbeldam, D.; Vlugt, T. J. H. *J. Phys. Chem. C* **2011**, *115*, 15355–15360.

(35) Zimmermann, N. E. R.; Jakobtorweihen, S.; Beerdsen, E.; Smit, B.; Keil, F. J. *J. Phys. Chem. C* **2010**, *114*, 15546.

(36) Kärger, J.; Demontis, P.; Suffritti, G. B.; Tilocca, A. *J. Chem. Phys.* **1999**, *110*, 1163–1172.

(37) Peters, B.; Zimmermann, N. E. R.; Beckham, G. T.; Tester, J. W.; Trout, B. L. *J. Am. Chem. Soc.* **2008**, *130*, 17342–17350.

(38) Schüring, A.; Auerbach, S. M.; Fritzsche, S. *Chem. Phys. Lett.* **2007**, *450*, 164–169.

(39) Haranczyk, M.; Sethian, J. A. *J. Chem. Theory Comput.* **2010**, *6*, 3472–3480.

(40) Lin, L.-C.; Berger, A. H.; Martin, R. L.; Kim, J.; Swisher, J. A.; Jariwala, K.; Rycroft, C. H.; Bhown., A. S.; Deem, M. W.; Haranczyk, M.; Smit, B. *Nat. Mater.* **2012**, *11*, 633–641.

345

Table of Contents Graphics

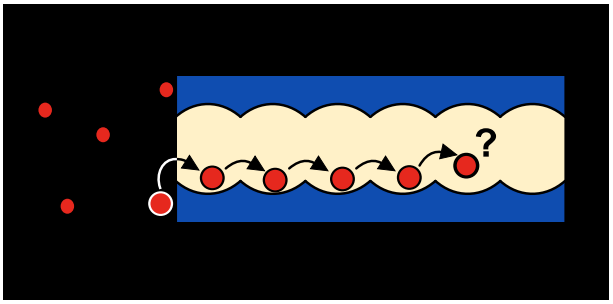

346